Hindawi
International Journal of Photoenergy
Volume 2021, Article ID 1961134, 14 pages
https://doi.org/10.1155/2021/1961134

Research Article

Optimum Height and Tilt Angle of the Solar Receiver for a 30 kWe Solar Tower Power Plant for the Electricity Production in the Sahelian Zone

Kory Faye,[1] **Ababacar Thiam**,[1,2] **and Mactar Faye**[1,2]

[1]*Efficiency and Energetic Systems Research Group, Alioune Diop University of Bambey, BP 30, Senegal*
[2]*Applied Energy Laboratory, Polytechnic School, Cheikh Anta Diop University of Dakar, BP 5085 Dakar Fann, Senegal*

Correspondence should be addressed to Kory Faye; kory.faye@uadb.edu.sn

Received 20 April 2021; Accepted 5 July 2021; Published 22 July 2021

Academic Editor: Leonardo Sandrolini

This work investigated the prediction of the optimum height and tilt angle of the solar receiver of a 30 kWe solar tower power plant for the electricity production in the Sahelian zone. Initially, the solar field is sized to determine the total reflecting surface area of the mirrors and the number of heliostats. A PS10-like radially staggered heliostat field is used to design the heliostat layout in the field using a Matlab code. The concentrated solar flux at the input of the receiver was determined using Soltrace software by the Monte Carlo ray tracing (MCRT) method. The sizing results show that the total reflecting surface area is 350 m^2 for an optical efficiency of 76.4% and a reference DNI of 600 W/m^2. The solar field layout indicates 175 heliostats of 2 m^2 surface area and 1.5 m height each. The simulation results show that the optimum height and tilt angle of the solar receiver are 26 m and 65°, respectively.

1. Introduction

The increasing use of renewable energy sources to reduce the use of fossil fuels is an essential path for the transition to a sustainable energy future with low carbon emissions [1]. Solar energy is considered the most viable renewable energy source in areas with high solar potential [2]. It can be converted into electricity in two different ways: photovoltaic (PV) and concentrating solar power (CSP) technologies [3]. The manufacture of photovoltaic technology is expensive and hardly exists in Africa. Thus, CSP technology is considered as one of the promising ways for future sustainable electricity production [4]. Among the CSP technologies, solar tower power plants (STPP) present the best performance due to their capacity to provide high temperatures and therefore high efficiency [5]. The STPP technology can be also hybridized with other energy sources and have the ability to store heat [6].

In many African countries, in particular the Sahelian zone has significant potential for the installation of STPP due to strong direct solar irradiation (DNI) of between 1400 and 2000 kWh/m^2/year [7]. In addition, the electrification rate in the sub-Saharan zone is around 32% [8] on average with a strong variation from one country to another. This rate is much lower in rural areas (16%) where around 70% of the population lives [8]. The use of STPP technology can decrease this low electrification rate.

The solar field represents the key subsystem of the STPP because it contributes around 50% [9] of the total cost of the plant and causes 40% [10] of the overall energy losses. So the performance of a solar STPP depends strongly on the solar field efficiency [11]. Indeed, the solar field efficiency depends mainly on the heliostat layout in the field, the tracking system, and the control systems [11]. The optimization of heliostat layout can reduce energy losses and therefore maximize the concentrated solar flux at the input of the receiver.

Many researchers have been interested in the different categories of the heliostat layout of the solar field to find the optimal layout. Wei et al. [12] have experimented and optimized four models of heliostat field layout including north-south cornfield, north-south stagger, radial cornfield, and radial stagger. They conclude that the north-south cornfield layout is the optimal decision for the 1 MWe STPP. Zhou and Zhao [13] have presented a new method of

heliostat field layout design for two typical models: cornfield and radial stagger. The results showed an optical efficiency of 82.5% and a ground coverage of 33.6% for the radial stagger against an optical efficiency of 86.3% and a coverage of 38.3% for the cornfield. Lipps and Vant-Hull [14] have presented four categories of heliostat field layout: radial cornfield, radial stagger, north-south cornfield, and north-south stagger for a 100 MWe central receiver system. The results showed that radial staggers are better than cornfield because they reduce the field area and increase the concentrated solar flux.

In addition, several parameters affecting the heliostat layout have been developed and optimized for maximizing concentrated solar flux. Siala and Elayeb [15] have presented a graphical method for the radial stagger layout. The heliostats are divided into groups and rings while respecting the principle of no-blocking, the safety distance (d_s), and the area density criteria. This method is also represented by mathematical equations thus facilitating its computer implementation. Collado [16] has developed a radial stagger layout for surrounded heliostat field which only uses two parameters for optimization, i.e., a no-blocking factor and safety distance. He confirmed that this method needs some improvement to find the optimal mean radial (ΔR) and azimuthal spacing of the heliostat field. Wei et al. [17] have proposed a new method for designing the heliostat field layout for a STPP. The heliostat boundary is constrained by the receiver aperture (acceptance angle (δ_r) and opening radius (R_{out})) and the efficiency factor. They showed that the design time is reduced when calculating the concentrated solar flux. Zhang et al. [18] have defined a new factor called efficiency of available land. This factor is a function of atmospheric attenuation losses (η_{att}) and spilling losses (η_{spil}). It was used to position in an optimum way the heliostats of a 1 MW STPP. Its performance shows an annual optical efficiency (η_{opt}) of 71.36%. Collado and Guallar [19] have presented the details of the optimization of a large STPP like Noor III (150 MWe, 7400 heliostats) performed with the campo code [20]. They demonstrated that this code is able to optimize the heliostat field with only two parameters: the minimum (ΔR_{min}) and maximum (ΔR_{max}) radial spacing. This article [21] analyzes the site slope effect on the optical efficiency (η_{opt}) of the solar field. Latitude (λ) is treated as a control variable since it modifies all the field characteristics solar. This study reveals that choosing the optimal site improves optical efficiency by up to 1.65%.

The above research works are concerned with different types of heliostat layouts in the solar field and the parameters involved in the design of any heliostat layout. To our knowledge, no study has yet been carried out to assess the influence of the height and tilt angle of the solar receiver on the concentrated solar flux. The objective of the present study is to determine the optimum height and tilt angle of the solar receiver of a 30 kWe STPP intended for the production of electricity in the Sahelian zone.

To achieve this objective, the solar field is firstly sized to determine the total reflective area of the heliostats and the number of heliostats. Then, a calculation code is developed in Matlab software to determine the heliostat layout and the positions and orientations of each heliostat. Finally, we have varied the height and tilt angle of the solar receiver to determine the peak flux.

2. Materials and Methods

2.1. Solar Field Sizing. The sizing of the solar field is done by determining the total reflecting area (A_T) of the heliostats. The method described in Figure 1 is suitable [4]. It consists of determining the total reflective area of the heliostats from the electrical power (E_p) of the STPP. This area can be determined by the following expression [4]:

$$A_T = \frac{E_p}{\eta_{opt} \cdot \eta_{rec} \cdot \eta_{conv} \cdot \mathrm{DNI}}, \quad (1)$$

where η_{opt} is the optical efficiency of the heliostat, η_{rec} is the solar receiver efficiency, η_{conv} is the conversion yield, and DNI is the direct normal irradiation in the local area.

The optical efficiency (η_{opt}) of the heliostats reflects the quantity of energy reaching the receiver following the reflection of solar rays by the heliostats [12]. It determines the set of field losses such as atmospheric attenuation (η_{aat}), cosine (η_{cos}), shading and blocking ($\eta_{sh\&bloc}$), reflecting (η_{ref}), and spilling losses (η_{spil}) [22].

$$\eta_{opt} = \eta_{aat} \cdot \eta_{cos} \cdot \eta_{sh\&bloc} \cdot \eta_{ref} \cdot \eta_{spil}. \quad (2)$$

The cosine losses represent the cosine of the angle between the incident solar ray and the vector normal to the reflecting surface of the heliostat. Therefore, they depend on both the position of the sun and the heliostat [23]. Atmospheric attenuation losses depend on weather conditions and the distance between the heliostats and the solar receiver [12]. Shading and blocking losses represent the phenomenon whereby concentrated solar rays are blocked by adjacent heliostats during scattering [24]. Spilling losses occur when the receiver cannot intercept all of the solar rays reflected by the heliostats.

The receiver efficiency (η_{rec}) is defined as the net thermal power absorbed compared to the total power intercepted at the input of the receiver. Therefore, in this definition is included the absorption losses (η_{ab}) and the conduction (η_{cond}), convection (η_{conv}), and radiation (η_{rad}) losses (see equation (3)) [4]. The conversion yield (η_{con}) of the power unit is composed of the electric efficiency (η_{turb}) of the micro gas turbine and the electrical generator efficiency (η_G) (see equation (4)) [4].

$$\eta_{rec} = \eta_{ab} \cdot \eta_{cond} \cdot \eta_{conv} \cdot \eta_{rad}, \quad (3)$$

$$\eta_{con} = \eta_{turb} \cdot \eta_G. \quad (4)$$

2.2. Heliostat Layout Design. Among the various heliostat layout designs mentioned above, we have adapted the radial stagger layout. This method minimizes the shading and blocking losses ($\eta_{sh\&bloc}$) and represents the most widespread layout [15]. For this, the limit of the solar field shown in Figure 2 is a function of the tower's height (h_T) and the

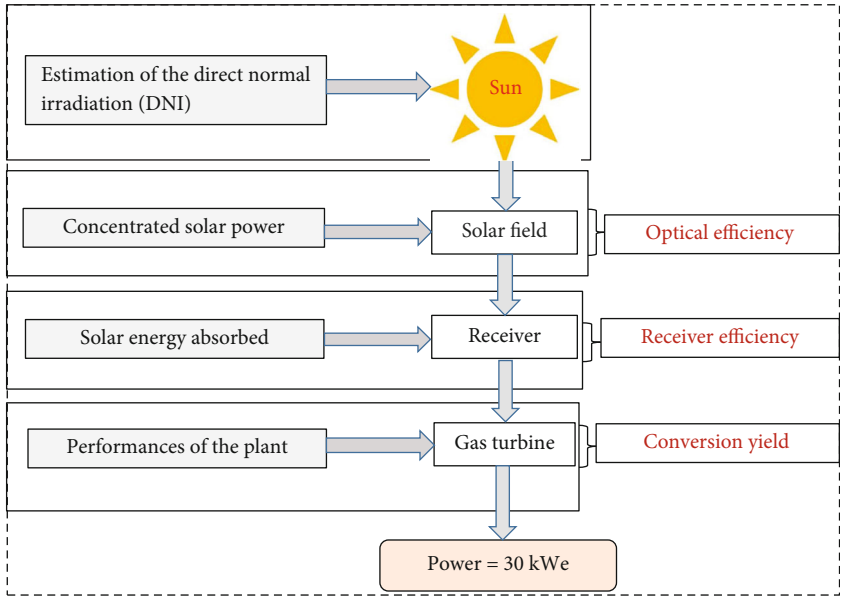

Figure 1: Sizing principle of a solar tower power plant.

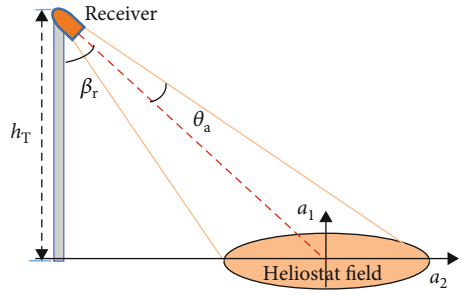

Figure 2: Projection limit on the field from the opening of the solar receiver.

geometry of the solar receiver (acceptance angle (θ_a), inlet diameter (R_{in}), and tilt angle (β_r)). The acceptance angle is defined as the maximum angle according to which any ray reflected from the solar field with an incident angle (θ) less than this can be received by the receiver [25]. The opening of the receiver is circular, and consequently, the limits of its projection on the solar field are described by an ellipse of semiminor axis (a_1) and semimajor axis (a_2) given by the following equations [26, 27]:

$$a_1 = \frac{h_T \cdot \tan(\theta_a) \cdot \left(1 + \tan^2(\theta_a)\right)}{1 - \tan^2(\beta_r) \cdot \tan^2(\theta_a)}, \tag{5}$$

$$a_2 = \frac{h_T \cdot \tan(\theta_a)}{1 - \tan^2(\beta_r) \cdot \tan^2(\theta_a)} \sqrt{\left(1 + \tan^2(\beta_r)\right) \cdot \left(1 + \tan^2(\beta_r)\, \tan^4(\theta_a)\right)}. \tag{6}$$

In the radial stagger layout, the heliostats are divided into groups, themselves distributed in numbered rings starting from the tower. The even rings are called the essential rings, and the odd rings are called the staggered rings. This method takes into account the tilt angle of the solar field (β_L). In this method, the trajectory of a heliostat is represented by a circle as shown in Figure 3(a). Its characteristic diameter (DM) given by equation (7) is equal to the diagonal (D) of the heliostat plus the interheliostat safety distance (d_s) [15].

$$\mathrm{DM} = D + d_s. \tag{7}$$

Using the dimensions of a heliostat, the characteristic diameter is written

$$\mathrm{DM} = \left(\sqrt{1 + f^2} + d_s\right) \cdot L_h, \tag{8}$$

where f is the ratio between the width and the length of the heliostat and L_h is the length of the heliostat.

2.2.1. Azimuthal Spacing. The azimuthal spacing in the first ring of each group representing the minimum spacing is equal to DM [15]. In the other rings, the azimuthal spacing is chosen while taking care of the principle of no-blocking. For any group j, the azimuth angle (γ_j) can be expressed by the following relation [15]:

$$\gamma_j = \frac{\mathrm{DM}}{2R_{i,j}}, \tag{9}$$

where $R_{i,j}$ represents the radius in a ring i and a group j.

The heliostats that have the same azimuth angle can be classified in the same group. The angular direction (Ψ_m) is an angle between the north axis and the distribution axes. It can be given by the following equation [15].

$$\Psi_m = \pm n \cdot \gamma_j, \tag{10}$$

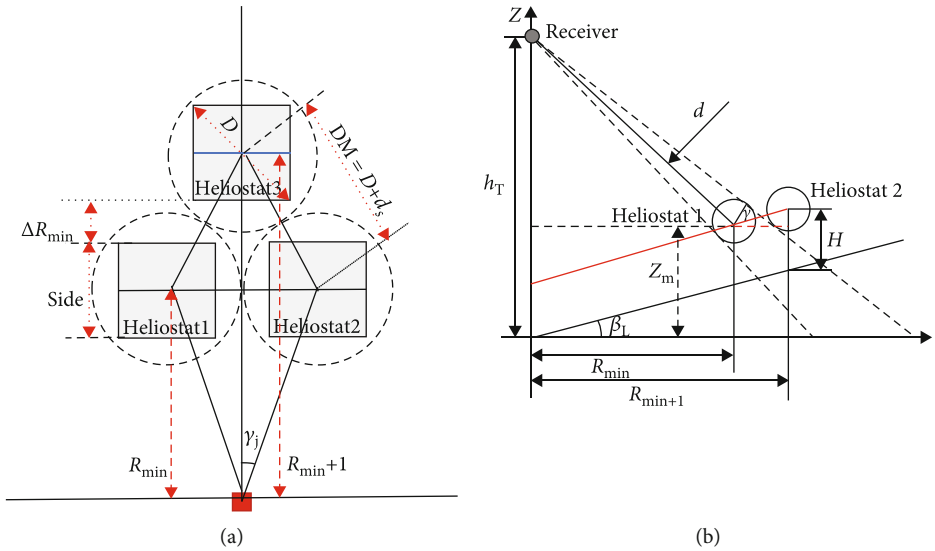

Figure 3: Parameters defining the design of the (a) heliostat and the (b) no-blocking principle.

where $n = 0, 2, 4, \cdots$, for the essential rings, $n = 1, 3, 5, \cdots$, for the staggered rings, + for the northeast half field, and − for the northwest half field.

2.2.2. Radial Spacing. The radius of each ring is determined by the nature of the ring. The radius of the first ring is generally given as a function of the receiver's height (h_T). The values proposed by Collado and Turegano [28] and Falcone [29] are generally between $h_T/2$ and h_T. We choose R_{min} such that

$$R_{min} = \frac{h_T}{2} + 1. \tag{11}$$

For the second ring in any group j, the radius can be expressed on a solar field inclined at an angle (β_L) by [13]

$$R_{min+1} = R_{min} + DM \cdot \cos(30) \cdot \cos(\beta_L). \tag{12}$$

So the minimum radial spacing (ΔR_{min}) between the heliostats can be given by

$$\Delta R_{min} = DM \cdot \cos(30) \cdot \cos(\beta_L). \tag{13}$$

The maximum radial spacing (ΔR_{max}) should be determined by equation (17) according to the principle of no-blocking between adjacent heliostats as shown in Figure 3(b). The detailed calculations of this principle are given by equations (14), (15), and (16) [13].

$$z_m = R_{min} \cdot \tan(\beta_L) + H_h, \tag{14}$$

$$d = \sqrt{R_{min}^2 + (h_T - z_m)^2}, \tag{15}$$

$$\gamma = \arcsin\left(\frac{DM}{2 \cdot d}\right) + \arcsin\left(\frac{R_{min}}{d}\right) - \beta_L, \tag{16}$$

$$\Delta R_{max} = \frac{DM \cdot \cos(\beta_L)}{\cos(\gamma)}. \tag{17}$$

Finally, the radius of the other rings can be determined by the following relation [13]:

$$R_{min+n} = R_{min} + \Delta R_{min} + R_{coef}(\Delta R_{max} - \Delta R_{min}), \tag{18}$$

where R_{coef} is the optimized coefficient of the radius.

2.3. Positions and Orientations of the Heliostats. The first step to find the position and the orientation of the heliostats in the solar field is to determine the position of the sun. The sun's position is characterized by the altitude (α) and the azimuth angle (A). Figure 4(a) shows the angles defining the apparent position of the sun. The sun's altitude is calculated as follows [30, 31]:

$$\alpha = \sin^{-1}(\sin(\lambda) \cdot \sin(\delta) + \cos(\delta) \cdot \cos(\lambda) \cdot \cos(\omega)), \tag{19}$$

where λ is the local latitude, δ is the solar declination angle, and ω is the hour angle. The solar declination angle (δ) depends on the day number (N) of the year and can be determined by [30]

$$\delta = 23,45 \sin \cdot \left(\frac{360}{365} \cdot (284 + N)\right). \tag{20}$$

The hour angle is measured from solar noon and is given by [30]

$$\omega = 15 \cdot (12 - TSV), \tag{21}$$

where TSV is the solar time. Then, the solar azimuth angle (A) representing the angle between the projection of the sun's direction and the north direction is given by [30]

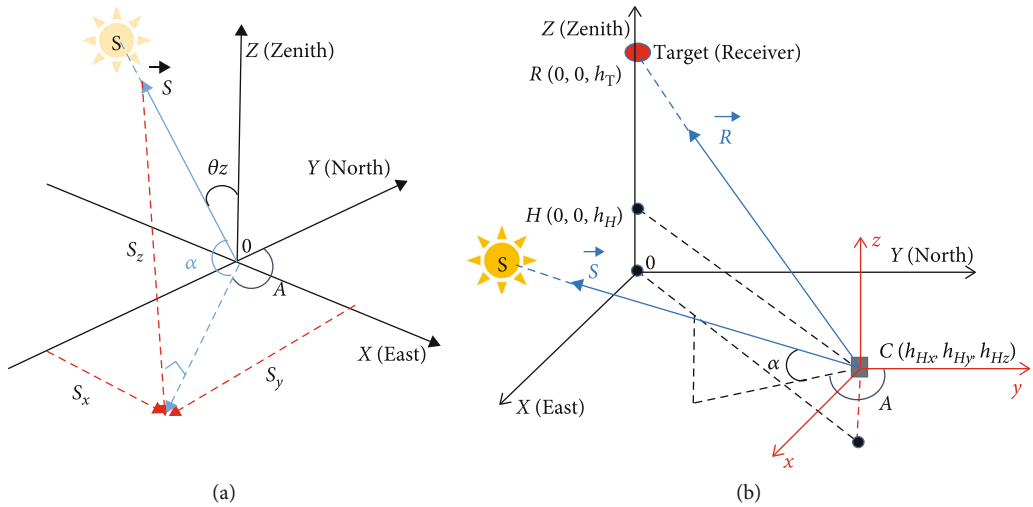

Figure 4: Positions of the (a) sun and the (b) heliostat.

$$A = \arcsin\left(\frac{\cos(\delta)\cdot\sin(w)}{\cos(\alpha)}\right). \tag{22}$$

The sun vector $(\vec{S})$, as illustrated in Figure 4(b), can be defined by equation (23) where $\vec{i}$, $\vec{j}$, and $\vec{k}$ represent, respectively, the unit vectors of the x, y, and z axes.

$$\vec{S} = S_x\vec{i} + S_y\vec{j} + S_z\vec{k}. \tag{23}$$

By projection in the frame (O, i, j, k), the three components (S_x, S_y, S_z) of the sun vector are determined as follows [32]:

$$S = \begin{cases} S_x = \cos(\alpha)\cdot\sin(A), \\ S_y = \cos(\alpha)\cdot\cos(A), \\ S_z = \sin(A). \end{cases} \tag{24}$$

A heliostat is located in the solar field by the coordinates of its center (see Figure 4(b)) which are determined once the angular direction (Ψ_m) of the heliostat and the radius (R) of the ring to which it belongs are known. Thus, the coordinates (H_x, H_y, H_z) of each heliostat can be determined by the following system of equations [13]:

$$H = \begin{cases} H_x = R\cdot\sin(\Psi_m), \\ H_y = R\cdot\cos(\Psi_m), \\ H_z = H_h. \end{cases} \tag{25}$$

The cosine losses (η_{cos}) which represents the greatest loss in the solar field is due to the angle between the incident solar ray and the normal vector at the heliostat's area. Therefore, it depends on both the position of the heliostat and the sun. To determine the normal vector $(\vec{n})$ at the heliostat's area, the vector $(\vec{R})$ located between the solar receiver and the heliostat must be defined first [33].

$$\vec{R} = \frac{\vec{T} - \vec{C}}{\left\|\vec{T} - \vec{C}\right\|}, \tag{26}$$

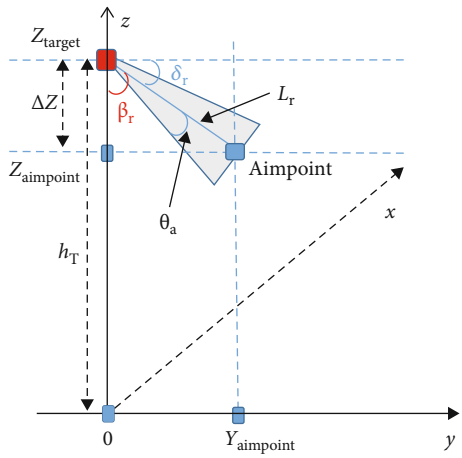

Figure 5: Method for determining the tilt angle of the solar receiver.

Table 1: Various estimated efficiency factors.

Characteristics	Parameters	Values	Ref.
Efficiency factors	η_{aat}	0.95	[32]
	η_{cos}	0.90	[4]
	$\eta_{sh\&.bloc}$	0.95	[32]
	η_{ref}	0.97	[34]
	η_{spil}	0.97	[4]
Conversion yield	η_{turb}	0.26	[35]
	η_G	0.90	[36]
Receiver	η_{rec}	0.80	[37]

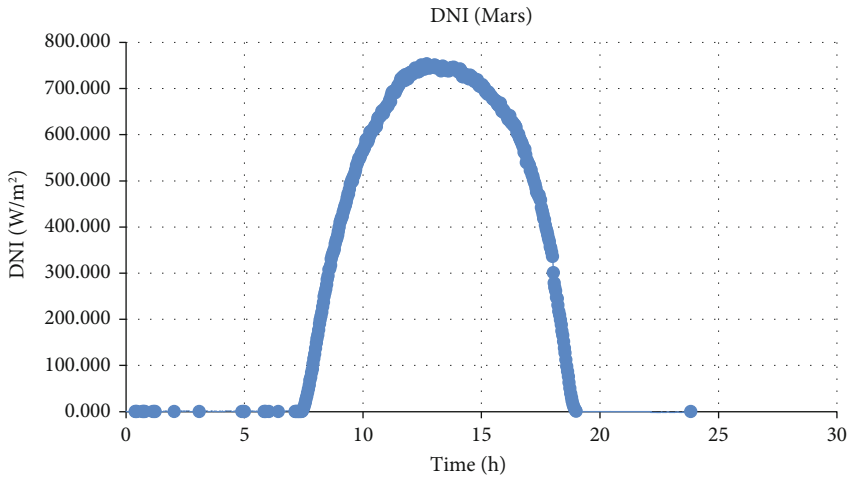

Figure 6: Daily profiles of DNI of March 21 in Senegal.

where $\vec{T}$ and $\vec{C}$ represent, respectively, the position vectors of the sun and the heliostat. Thus, the normal vector ($\vec{n}$) at the heliostat's area is given by [23]

$$\vec{n} = \frac{\vec{R} + \vec{S}}{\sqrt{2 \cdot \left(1 + \vec{S}.\vec{R}\right)}}. \quad (27)$$

Then, the target vector ($\vec{N}$) which determines the heliostat's position and orientation is given by

$$\vec{N} = \vec{H} + \vec{n}. \quad (28)$$

2.4. Tilt Angle of the Receiver. The method described in Figure 5 is used to determine the optimum tilt angle of the solar receiver. This method consists of calculating the coordinates of the receiver, i.e., Aimpoint (X_{aimpoint}, Y_{aimpoint}, and Z_{aimpoint}) for different tilt angles of the solar receiver. The system of equations given by the following relation calculates the coordinates of the receiver for each tilt angle.

$$\text{Aimpoint} = \begin{cases} X_{\text{ap}} = 0, \\ Y_{\text{ap}} = L_{\text{r}} \cdot \cos\left(\delta_{\text{r}}\right), \\ Z_{\text{ap}} = Z_{\text{target}} - \Delta Z, \end{cases} \quad (29)$$

where Z_{target} is the height of the tower, L_{r} is the length of the solar receiver, and $\Delta Z = L_{\text{r}} \cdot \sin\left(\delta_{\text{r}}\right)$.

2.5. Operating Parameters. We estimated the different efficiency factors that determine optical efficiency (η_{opt}). We have also chosen the various factors that participate in the sizing of the solar field such as the solar receiver efficiency (η_{rec}), the turbine efficiency (η_{turb}), and the electric generator efficiency (η_{G}). All of its operating parameters are provided in Table 1.

Table 2: Characteristics of solar field subsystems.

Subsystems	Parameters	Values	Units
Heliostats	Form	Square	[-]
	Number	175	[-]
	Height	1.50	[m]
	Area	2	[m^2]
	Reflectivity	0.90	[-]
	Transmittivity	0	[-]
Tower	Orientation	North	[-]
Receiver	Type	Volumetric	[-]
	Acceptance angle	25	[°]
	Transmittivity	0.90	[-]
	Reflectivity	0	[-]
	Length	1	[m]
	Opening radius	0.70	[m]
	Opening area	1.54	[m^2]

3. Results and Discussion

3.1. DNI Estimate. In this study, we used direct normal irradiation (DNI) data measured in Senegal. This data is available for one year, which is acceptable for the concentrating solar power (CSP) technologies. From these data, we chose those of March 21, which corresponds to the spring equinox where the sun passes at the zenith (i.e., vertical instead). The profile of the DNI for the day of March 21 is shown in Figure 6. For the sizing of the 30 kWe solar tower power plant, we chose a reference DNI of 600 W/m^2. This choice made it possible to obtain a solar operating range of 6 h.

3.2. Result of the Sizing. For the sizing of the solar field, we chose an indirect pressurized air volumetric solar receiver with an efficiency (η_{rec}) of 80% [37], a Capstone turbine (C30) with an electrical efficiency (η_{turb}) of 26% [35], and an electric generator (η_{G}) yield of 90% [36]. The results showed that the optical efficiency (η_{opt}) of the solar field is

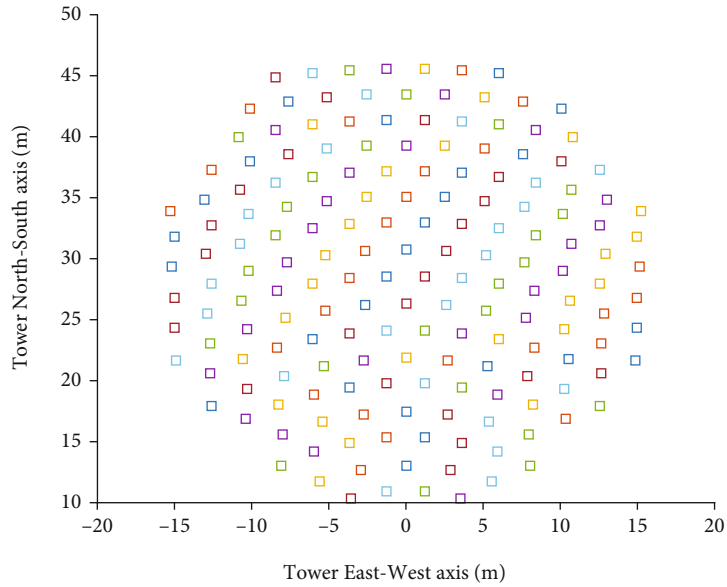

(a) Height of the solar tower = 20 m

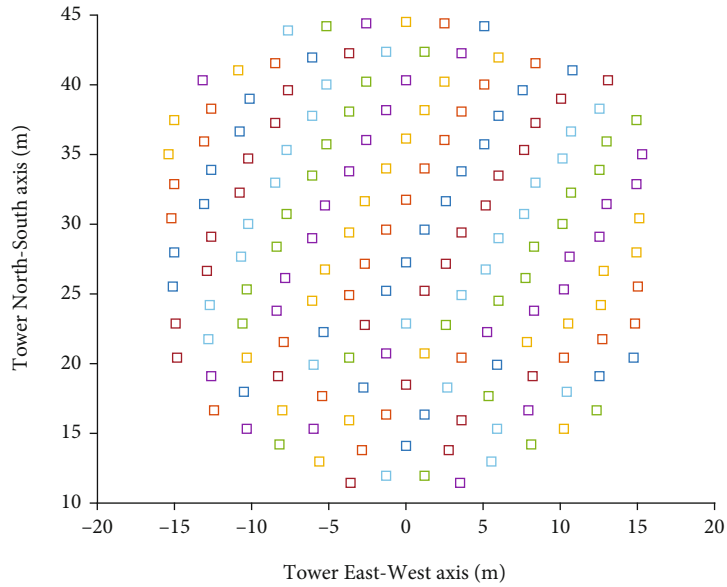

(b) Height of the solar tower = 22 m

Figure 7: Continued.

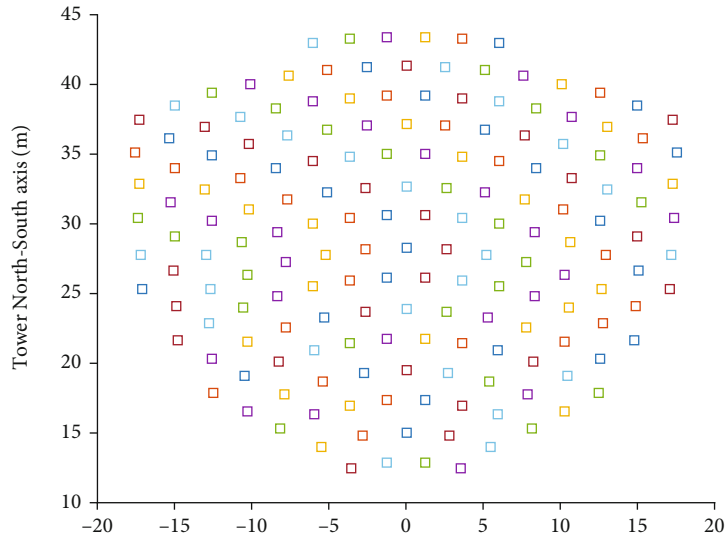

(c) Height of the solar tower = 24 m

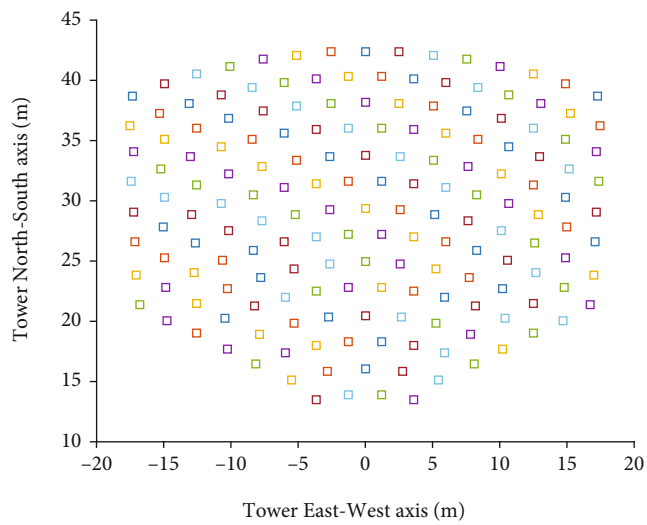

(d) Height of the solar tower = 26 m

Figure 7: Continued.

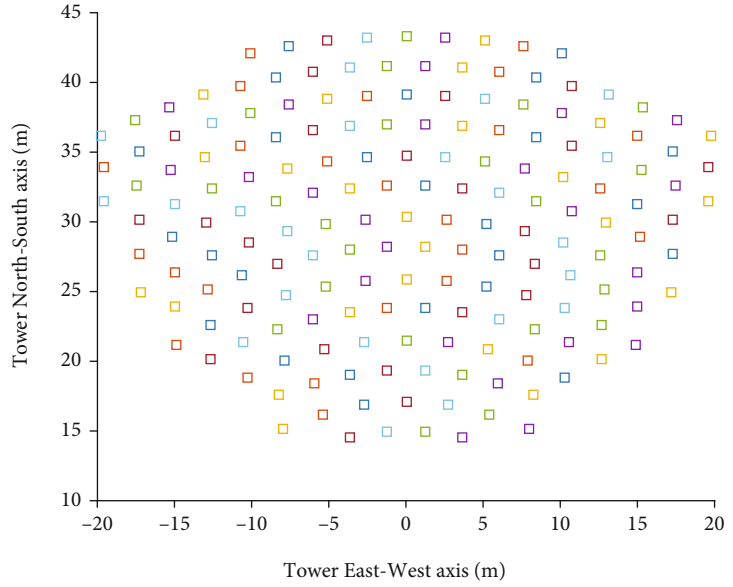

(e) Height of the solar tower = 28 m

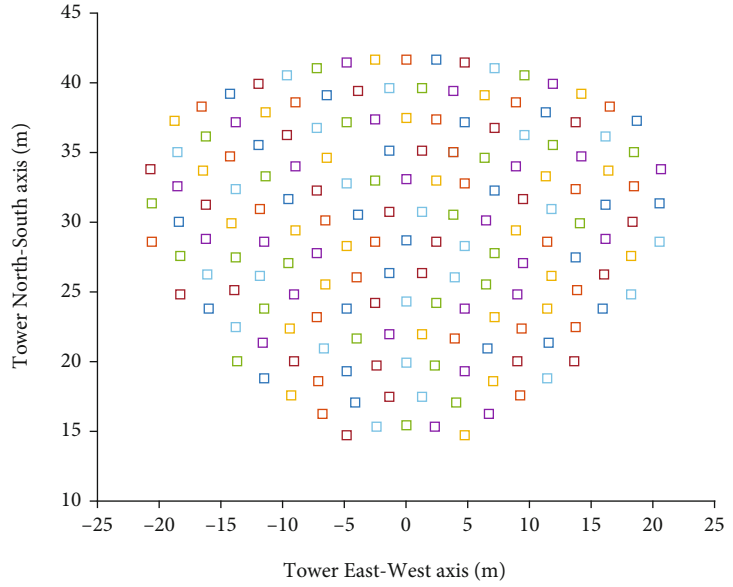

(f) Height of the solar tower = 29 m

Figure 7: Layouts of the solar field for different heights of the tower.

76.4% and the total reflecting area (A_T) of the heliostats is 350 m^2.

The size of the heliostats in solar tower power plants is relatively large (121 m^2 at PS10 and PS20) [38]. This large size of the heliostats increases mechanical stress, wind resistance, and production costs. Therefore, in this study, we chose small heliostats that could easily be handled for upkeep and maintenance. The chosen mini heliostats have a reflecting area of 2 m^2 and a height of 1.5 m. The surface shape of the heliostat mirror is square. So the solar field is composed by 175 heliostats. The site for the installation of the solar tower power plant is located in the department of Podor (Saint-Louis, Senegal) where the north latitude is about 16° 40′ and the west longitude is about 14° 57′.The solar field is a horizontal plane and is tilted 0° with respect to the solar receiver. The main characteristics of the solar field subsystems are provided in Table 2.

3.3. Heliostat Layout Results. The radial stagger layout of the solar field shown in Figure 7 is designed for the 30 kWe STPP. The heliostats are placed north of the tower in the solar field. For an interheliostat security factor (ds) of 0.3, the characteristic diameter (DM) of the heliostats is 2.42 m. The minimum (ΔR_{min}) and maximum (ΔR_{max}) radial spacing between the heliostats are 2.1 m and 2.45 m, respectively, for the optimized coefficient of the radius (R_{coef}) of 0.6. The coordinates of each heliostat, the azimuth angle (γ_j), and the radius (R) of each ring are calculated. Figure 7 shows

Table 3: Characteristics of each heliostat layout design.

Heights of the tower	20 m	22 m	24 m	26 m	28 m	29 m
Semiminor axis a_1 (m)	15.14	15.96	17.41	18.86	20.31	21.04
Semimajor axis a_2 (m)	18.72	18.97	20.69	22.42	24.15	25.01
Field area (m^2)	890.5	951.3	1132.1	1328.6	1540.9	1652.9
Number of rings	17	16	15	14	14	13
Essential rings	9	8	8	7	7	6
Staggered rings	8	8	7	7	7	7
Radius of the first ring (m)	11	12	13	14	15	15.5
Radius of the last ring (m)	45.68	44.56	43.44	42.33	43.32	41.72

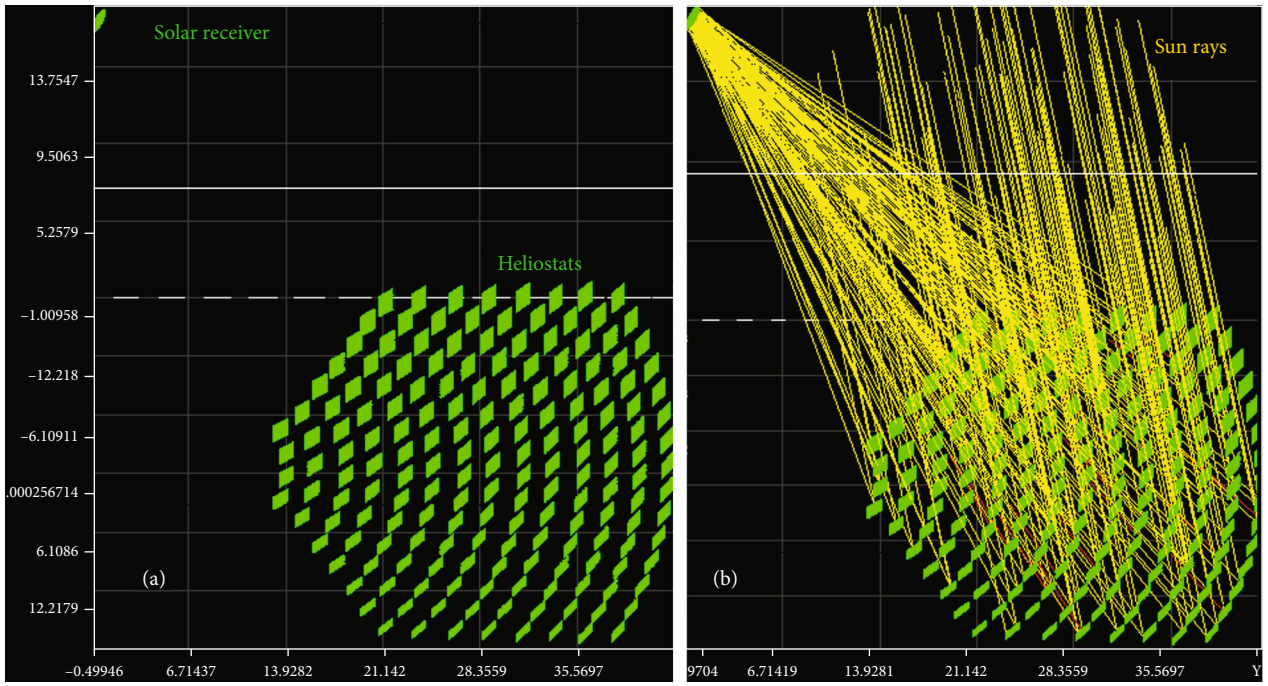

Figure 8: Design of (a) heliostat layout and (b) visualization of rays in Soltrace.

the heliostat layout in the solar field for the heights (h_T) of 20 m, 22 m, 24 m, 26 m, 28 m, and 29 m. The characteristics of each heliostat layout are given in Table 3.

As can be clearly seen in Table 3, the semiminor (a_1) axis and the semimajor (a_2) axis increase with the height of the tower, which leads to an increase in the solar field area. However, the number of rings decreases as the height of the tower increases. This shows that the more of field area increases, the number of heliostats in a ring is high, and therefore, the number of rings decreases. The radius of the first ring depends on the tower height and that of the last ring depends not only on the tower height but also on the number of rings.

3.4. Simulation Results. After calculating the parameters of each heliostat and their design over the field using Matlab software, an Excel file is generated indicating all the positions and orientations of the heliostats. This card is incorporated in Soltrace to indicate the positions of the heliostats, the tower, and the solar receiver as illustrated in Figure 8(a). Modelling and simulation of the solar field under Soltrace reproduce the trajectory of the solar rays and establish the concentrated flux map at the entrance of the receiver. Soltrace software takes into account the reflectivity (ρ_{ref}) of the mirrors and adjustment errors such as slope error (σ_{slope}) and specularity error (σ_{sp}). Assuming that the reflectivity of the mirror equals to 0.90, the transmittivity equals to 0, the slope error equals to 0.95 mrad, and the specularity error equals to 0.3 mrad. The solar receiver transmittivity is 0.90, the reflectivity is 0, the slope error is 0.9 mrad, and the secularity error is 0.2 mrad. For simulation, we launched 1,000,000 solar rays to visualize the energy flow at the input of the solar receiver. Figure 8(b) shows the visualization in the Soltrace environment of the intersections between the solar rays and the elements of the solar field (heliostats, solar receiver, and tower).

The solar flux distribution over the opening of the receiver is shown in Figure 9(a). As can be seen in this figure, the spilling losses are almost zero for an input radius (R_{in}) of the receiver of 0.7 m. With a direct normal irradiation (DNI)

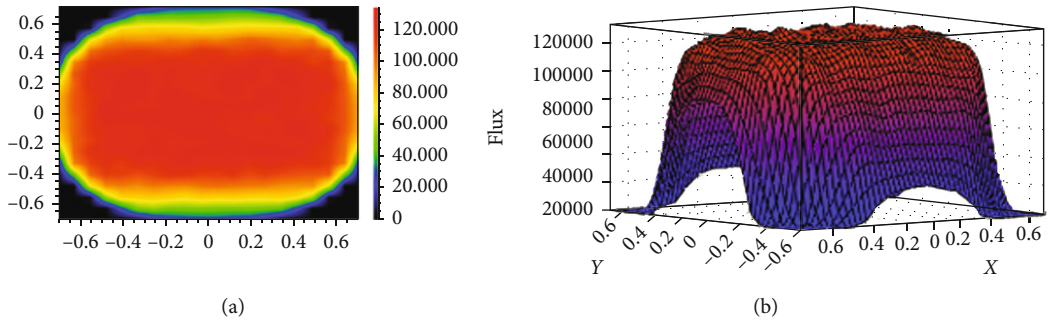

Figure 9: (a) Distribution of the solar flux at the input of the receiver and (b) the 3D flux map.

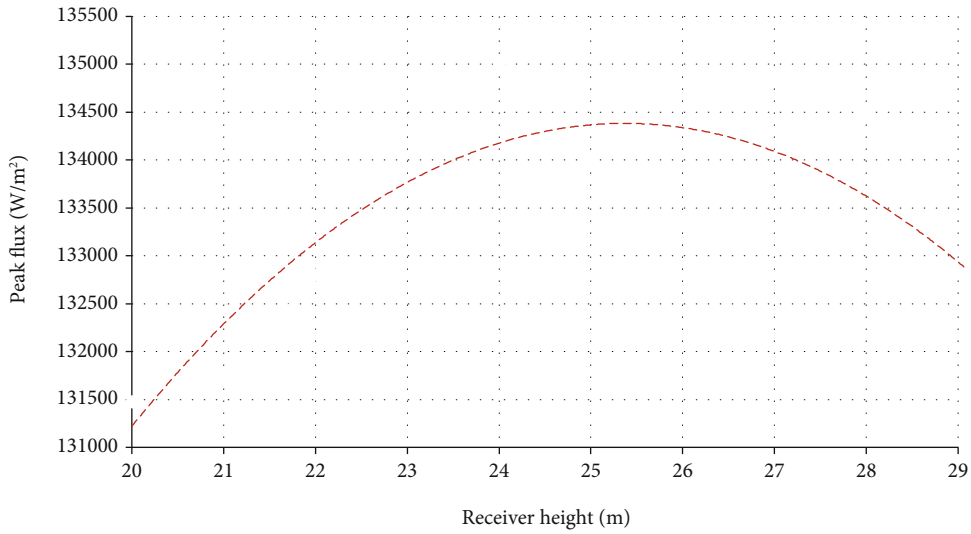

Figure 10: Maximum solar flux depending on the height of the tower.

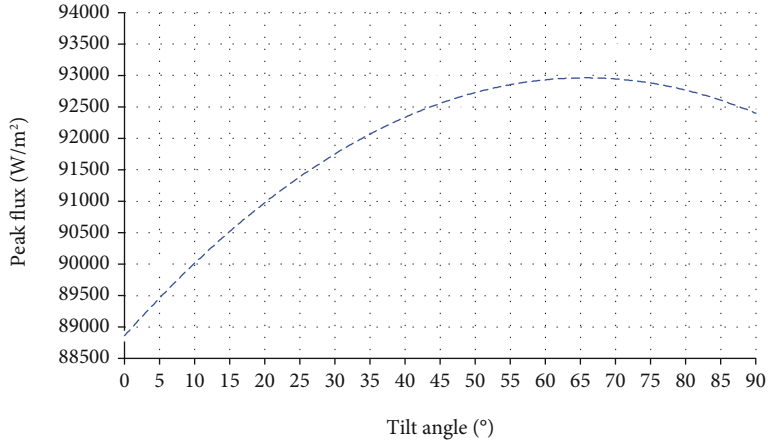

Figure 11: Maximum solar flux depending on the tilt angle of the receiver.

of 850 W/m^2, the maximum concentrated solar flux at the input of the receiver is approximately 120 kW/m^2 (i.e., 184.8 kW). Figure 9(b) shows the three-dimensional (3D) flux map which clearly shows the maximum solar flux.

We studied the influence of the tower's height (h_T) on the concentrated solar flux at the input of the solar receiver located at the top of the tower. For this, we varied the tower's height from 20 to 29 m to generate the maximum solar flux (peak flux) at the input of the solar receiver. The simulation results are shown in Figure 10. As we can clearly see from this figure, the solar flux starts to increase from 131.25 kW/m^2 for a height of 20 m up to about 134.40 kW/m^2 for a height of 26 m where it begins to decrease. In this interval (20 to 26 m), the solar receiver increasingly intercepts all of the solar

rays reflected by the heliostats. But after 26 m, the spilling losses (η_{spil}) seem to appear because the solar receiver is no longer able to intercept all the concentrated solar rays. These results made it possible to choose the height of the tower of 26 m because it allows obtaining a maximum solar flux at the input of the receiver which is approximately 134.4 kW/m^2.

The influence of the tilt angle (β_r) of the solar receiver on the concentrated solar flux is also studied in this work. The solar receiver's height (h_T) is 26 m, since it is the optimum value calculated previously. We varied the tilt angle from 0 to 90° to determine the maximum solar flux (peak flux). Figure 11 shows the simulation results obtained. The tendency is similar for the solar receiver's height. We note an increase in the solar flux up to values between approximately 60 and 65°. After 65°, the decrease of the peak flux is pronounced. This decrease is caused by the spilling losses (η_{spil}) at the opening of the solar receiver. In addition, due to the fact that the cosine losses (η_{cos}) and atmospheric attenuation losses (η_{att}) increase, these also lead to the decrease of the concentrated solar flux. The tilt angle is therefore an important parameter of the solar receiver which must be well chosen when it is desired to obtain the maximum solar flux. With these results, it can be concluded that the optimum tilt angle is approximately 65° which corresponds to the maximum solar flux equals to 93 kW/m^2 (143.22 kW).

4. Conclusion

The solar tower power plant offers interesting potential for the production of electricity in the Sahelian zone where the solar potential is high and the electrification rate remains low. The objective of this study was to determine the optimum height and tilt angle of the solar receiver of a 30 kWe STPP intended for the production of electricity in the Sahelian zone. The sizing of the solar field had given the following results: an optical efficiency of 76.4% for a reference DNI of 600 W/m^2, a total reflective area of the heliostats of 350 m^2, and a number of heliostats of 175 of 2 m^2 area and 1.5 m height. The simulation results showed that the optimum height and tilt angle of the solar receiver were 26 m and 65°, respectively.

These results will serve as a basis for the sizing of the compound parabolic concentrator (CPC) and the modelling of heat transfers within the solar receiver.

Nomenclature

A_T: Total reflecting surface area (m^2)
E_p: Electrical power (kWe)
a_1: Semiminor axis (m)
a_2: Semimajor axis (m)
h_T: Height of the tower (m)
L_h: Length of the heliostat (m)
R: Radius of the ring (m)
H_h: Height of the heliostat (m)
N: Day number of the year
L_r: Length of the receiver (m)
R_{out}: Output radius of the solar receiver (m)
R_{in}: Input radius of the solar receiver (m)
η_{opt}: Optical efficiency of the heliostat
η_{rec}: Solar receiver efficiency
η_{conv}: Conversion yield
η_{aat}: Atmospheric attenuation losses
η_{cos}: Cosine losses
$\eta_{sh\&bloc}$: Shading and blocking losses
η_{ref}: Reflecting losses
η_{spil}: Spilling losses
η_{ab}: Absorption heat losses (W/m^2)
η_{cond}: Conduction heat losses (W/m^2)
η_{conv}: Convection heat losses (W/m^2)
η_{rad}: Radiation heat losses (W/m^2).

Greek Symbols

η: Efficiency
β_r: Tilt angle of the receiver (°)
θ_a: Acceptance angle (°)
β_L: Solar field angle (°)
γ: Azimuthal angle of heliostats (°)
Ψ: Angular direction (°)
λ: Local latitude (°)
α: Altitude of the sun (°)
δ: Azimuth of the sun (°)
ω: Hour angle (h)
σ_{sp}: Specularity error (mrad)
σ_{slope}: Slope error (mrad)
ρ_{ref}: Reflectivity.

Abbreviations

DNI: Direct normal irradiation (W/m^2)
DM: Characteristic diameter (m)
TSV: Solar time
HFLD: Heliostat field layout design
STPP: Solar tower power plant
CSP: Concentrated solar power
PV: Photovoltaic
MTG: Micro gas turbine
CPC: Compound parabolic concentrator
MCRT: Monte Carlo ray tracing.

Data Availability

We can make data available on request. If you wish to have the data used in this study, you can contact Mactar Faye at the address mactar.faye@uadb.edu.sn.

Conflicts of Interest

The authors declare no conflict of interest.

Acknowledgments

We thank the academic authorities of Alioune Diop University of Bambey for their support.

References

[1] C. N. Markides, "The role of pumped and waste heat technologies in a high-efficiency sustainable energy future for the UK," *Applied Thermal Engineering*, vol. 53, no. 2, pp. 197–209, 2013.

[2] O. Behar, A. Khellaf, and K. Mohammedi, "A review of studies on central receiver solar thermal power plants," *Renewable and Sustainable Energy Reviews*, vol. 23, pp. 12–39, 2013.

[3] A. B. Awan, M. Zubair, and K. V. V. C. Mouli, "Design, optimization and performance comparison of solar tower and photovoltaic power plants," *Energy*, vol. 199, pp. 117–450, 2020.

[4] K. E. N'Tsoukpoe, K. Y. Azoumah, E. Ramde et al., "Integrated design and construction of a micro-central tower power plant," *Energy for Sustainable Development*, vol. 31, pp. 1–13, 2016.

[5] E. Bellos and C. Tzivanidis, "Concentrating solar collectors for a tri-generation system: a comparative study," *Applied sciences*, vol. 10, no. 13, article 4492, 2020.

[6] O. Behar, "A novel hybrid solar preheating gas turbine," *Energy Conversion and Management*, vol. 158, pp. 120–132, 2018.

[7] A. Thiam, C. Mbow, M. Faye, P. Stouffs, and D. Azilinon, "Assessment of hybrid concentrated solar power-biomass plant generation Potential in Sahel: case study of Senegal," *Natural Resources*, vol. 8, no. 8, pp. 531–547, 2017.

[8] I. Onyeji, M. Bazilian, and P. Nussbaumer, "Contextualizing electricity access in sub-Saharan Africa," *Energy for Sustainable Development*, vol. 16, no. 4, pp. 520–527, 2012.

[9] G. J. Kolb, S. A. Jones, D. Gorman, R. Thomas, R. Davenport, and R. Lumia, *Heliostat Cost Reduction Study*, Sandia National Laboratories, Albuquerque, NM, USA, 2007.

[10] Z. A. Hussaini, P. King, and C. Sansom, "Numerical simulation and design of multi-tower concentrated solar power fields," *Sustainability*, vol. 12, pp. 2–22, 2020.

[11] E. Leonardi and B. D'Aguanno, "CRS4-2: a numerical code for the calculation of the solar power collected in a central receiver system," *Energy*, vol. 36, no. 8, pp. 4828–4837, 2011.

[12] X. Wei, Z. Lu, Z. Lin, H. Zhang, and Z. Ni, "Optimization procedure for design of heliostat field layout of a 1MWe solar tower thermal power plant," *Solid State Lighting and Solar Energy Technologies*, vol. 6841, pp. 1–19, 2008.

[13] Y. Zhou and Y. Zhao, "Heliostat field layout design for solar tower power plant based on GPU," in *Preprints of the 19th World Congress IFAC Cape Town*, South Africa, August 2014.

[14] F. W. Lipps and L. L. Vant-Hull, "A cellwise method for the optimization of large central receiver systems," *Solar Energy*, vol. 20, no. 6, pp. 505–516, 1978.

[15] F. M. F. Siala and M. E. Elayeb, "Mathematical formulation of a graphical method for a no-blocking heliostat field layout," *Renewable Energy*, vol. 23, no. 1, pp. 77–92, 2001.

[16] F. J. Collado, "Quick evaluation of the annual heliostat field efficiency," *Solar Energy*, vol. 82, no. 4, pp. 379–384, 2008.

[17] X. Wei, Z. Lu, Z. Wang, W. Yu, H. Zhang, and Z. Yao, "A new method for the design of the heliostat field layout for solar tower power plant," *Renewable Energy*, vol. 35, no. 9, pp. 1970–1975, 2010.

[18] H. Zhang, Z. Wang, X. Wei, and Z. Lu, "Design of heliostats field for scale of 1 MW solar power tower plant," *Procedia Environmental Sciences*, vol. 11, pp. 1164–1170, 2011.

[19] F. J. Collado and J. Guallar, "Quick design of regular heliostat fields for commercial solar tower power plants," *Energy*, vol. 178, pp. 115–125, 2019.

[20] F. J. Collado and J. Guallar, "A review of optimized design layouts for solar power tower plants with campo code," *Renewableand Sustainable Energy Reviews*, vol. 20, pp. 142–154, 2013.

[21] K. Lee and I. Lee, "Optimization of a heliostat field site in central receiver systems based on analysis of site slope effect," *Solar Energy*, vol. 193, pp. 175–183, 2019.

[22] C. J. Noone, M. Torrilhon, and A. Mitsos, "Heliostat field optimization: a new computationally efficient model and biomimetic layout," *Solar Energy*, vol. 86, no. 2, pp. 792–803, 2012.

[23] S. M. Besarati and D. Y. Goswami, "A computationally efficient method for the design of the heliostat field for solar power tower plant," *Renewable Energy*, vol. 69, pp. 226–232, 2014.

[24] J. Wang, L. Duan, Y. Yang, and L. Yang, "Rapid design of a heliostat field by analytic geometry methods and evaluation of maximum optical efficiency map," *Solar Energy*, vol. 180, pp. 456–467, 2019.

[25] L. Li, B. Wang, J. Pye, and W. Lipiński, "Temperature-based optical design, optimization and economics of solar polar-field central receiver systems with an optional compound parabolic concentrator," *Solar Energy*, vol. 206, pp. 1018–1032, 2020.

[26] A. Segal and M. Epstein, "Comparative performances of 'tower-top' and 'tower-reflector' central solar receivers," *Solar Energy*, vol. 65, no. 4, pp. 207–226, 1999.

[27] A. Segal, "Optimum layout of heliostat field when the tower-top receiver is provided with secondary concentrators," *Report for SFERA, WP.13, Task 2*, Weizmann Institute of Science, Israel, 2012.

[28] F. J. Collado and J. A. Turégano, "Calculation of the annual thermal energy supplied by a defined heliostat field," *Solar Energy*, vol. 42, no. 2, pp. 149–165, 1989.

[29] P. K. Falcone, *A Handbook for Solar Central Receiver Design*, Sandia National Laboratories, 1986.

[30] M. J. Reno, C. W. Hansen, and J. S. Stein, "Global Horizontal Irradiance Clear Sky Models: Implementation and Analysis," *Sandia Report SAND2012-2389*, U.S. Department of Energy's National Nuclear Security Administration, 2012.

[31] J. J. Ontiveros, C. D. Avalos, F. Loza, N. D. Galán, and G. J. Rubio, "Evaluation and design of power controller of two-axis solar tracking by PID and FL for a photovoltaic module," *International Journal of Photoenergy*, vol. 2020, Article ID 8813732, 13 pages, 2020.

[32] A. Giostri, M. Binotti, C. Sterpos, and G. Lozza, "Small scale solar tower coupled with micro gas turbine," *Renewable Energy*, vol. 147, pp. 570–583, 2020.

[33] T. Arrif, A. Benchabane, M. Guermoui, A. Gama, and H. Merarda, "Optical performance study of different shapes of solar cavity receivers used in central receiver system plant," *International Journal of Ambient Energy*, vol. 42, no. 1, pp. 81–95, 2021.

[34] K. Kalathakis, N. Aretakis, I. Roumeliotis, A. Alexiou, and K. Mathioudakis, "Simulation models for supporting the solar thermal power plant operator," *Energy*, vol. 167, pp. 1065–1073, 2019.

[35] M. C. Cameretti, "Modelling of a hybrid solar micro-gas turbine fuelled by biomass from agriculture product," *Energy Reports*, vol. 6, pp. 105–116, 2020.

[36] J. Nelson, N. G. Johnson, P. Doron, and E. B. Stechel, "Thermodynamic modeling of solarized microturbine for combined heat and power applications," *Applied Energy*, vol. 212, pp. 592–606, 2018.

[37] B. A. Ndiogou, A. Thiam, C. Mbow, P. Stouffs, and D. Azilinon, "Numerical analysis and optimization of an indirectly irradiated solar receiver for a Brayton cycle," *Energy*, vol. 166, pp. 519–529, 2019.

[38] J. B. Blackmon, "Heliostat size optimization for central receiver solar power plants," in *Concentrating Solar Power Technology*, K. Lovegrove and W. Stein, Eds., pp. 536–576, Woodhead Publishing, 2012.